SVPG: A pangenome-based structural variant detection approach and rapid augmentation of pangenome graphs with new samples

Heng Hu[1], Runtian Gao[1], Zhongjun Jiang[1], Shuqi Cao[3], Yadong Liu[3], Murong Zhou[1], Wentao Gao[1], Shengming Zhou[1], Tao Jiang [3,*], Guohua Wang[1,2,3*]

1 College of Life Sciences, Northeast Forestry University, Harbin 150000, China

2 College of Computer and Control Engineering, Northeast Forestry University, Harbin 150000, China

3 Faculty of Computing, Harbin Institute of Technology, Harbin 150001, China

* Correspondence to: ghwang@nefu.edu.cn; tjiang@hit.edu.cn

Abstract: Breakthrough advances in long-read sequencing technologies have opened unprecedented opportunities to study genetic variations through comprehensive pangenome analysis. However, the availability of structural variant (SV) calling tools that can effectively leverage pangenome information is limited. In addition, efficient construction of pangenome graphs becomes increasingly challenging with acquisition of larger number of samples. In this study, we present SVPG, an approach that leverages haplotype-resolved pangenome reference for accurate SV detection and rapid pangenome graph augmentation from long-read sequencing data. Compared to state-of-the-art SV callers, SVPG maintained superior overall performance across different coverages and sequencing technologies. SVPG also achieves notable improvements in calling rare and individual-specific SVs on both simulated and real somatic datasets. Furthermore, in a benchmark involving 20 samples, SVPG accelerated pangenome graph augmentation by nearly 10-fold compared to traditional augmentation strategies. We believe that this novel SVPG method, has the potential to revolutionize SV detection and serve as an effective and essential tool, offering new possibilities for advancing pangenomic research.

INTRODUCTION

Structural variants (SVs), defined as DNA sequence alterations larger than 50 base pairs (bp), encompass insertions, deletions, inversions, translocations, and duplications[1, 2]. Compared to

single nucleotide variants, SVs are fewer in number; however, their broader genomic impact often leads to more significant phenotypic changes[3, 4]. In clinical medicine, SVs are closely associated with numerous genetic diseases, cancers, and complex disorders, emerging as crucial molecular markers for disease diagnosis and treatment[5, 6]. Simultaneously, SVs play an irreplaceable role in revealing genome evolution and analyzing population genetic diversity, providing key insights into species evolution and population characteristics[7].

SV detection has primarily relied on single reference genome sequences as analytical benchmarks. However, traditional methods such as Sniffles2[8] and cuteSV[9] face a fundamental limitation: the single reference genome cannot comprehensively reflect the rich genetic variation within species. This issue is pronounced in highly polymorphic regions or population-specific sequences, often leading to reference bias[10-12]. This bias affects the accurate mapping of sample-specific sequences, thereby reducing SV detection reliability. The emergence of pangenomes offers a new solution to this challenge. By integrating genomic information from multiple representative individuals, pangenomes create a complete genetic variation map encompassing both shared sequences and population-specific variants[13-15]. This comprehensive genetic background significantly improves genome alignment accuracy, offering unique advantages in SV detection, particularly in complex variant regions. Recently, the Human Pangenome Reference Consortium (HPRC) successfully constructed the first human pangenome reference draft through sequencing and assembly of diverse global populations, establishing a solid foundation for improving SV detection accuracy and understanding human genetic diversity[14].

Beyond improving detection of known variants, *de novo* variant discovery within the pangenome makes capturing individual-specific variants more flexible and pangenome refinement more scalable. By utilizing pangenomes as backgrounds of genetic diversity, researchers can precisely identify rare variants absent from population-level data within a single genome. This fundamentally accelerates the discovery of rare SVs, especially those critical for detecting cancer-specific SVs. Furthermore, as genomic studies expand in scale, pangenome construction and maintenance face substantial computational challenges. When integrating new

samples into existing pangenomes, traditional approaches typically require re-execution of expensive *de novo* assembly and complex graph construction, with computational burden scaling superlinearly with sample numbers. In this context, rapidly and accurately discover sample-specific SVs from new samples and dynamically integrate pangenomes without complete reconstruction significantly reduces computational costs and accelerates iterative pangenome updates.

Although the utility of pangenomes for SV detection has been widely recognized, there is a lack of effective tools to fully leverage this advanced resource; existing tools have notable limitations. Early attempts, such as the pangenome-guided SV detection tool PanSVR[16] and several short-read-based genotypers[12, 17-19] demonstrate the potential of leveraging pangenomes for accurate SV detection and genotyping. However, these tools were primarily designed for short-read sequencing data, which inherently limits their ability to resolve large SVs. Recent developments such as SVarp[20] and miniSV[21] represent significant advances in *de novo* SV discovery from pangenome. SVarp can generate SV-related contigs through local assembly, while miniSV provides direct SV calling based on the pangenome graph. Both tools are still in the early stages of development, and their performance in diverse genomic contexts has yet to be evaluated comprehensively.

Here we present SVPG, a toolkit designed for SV detection and pangenome graph construction. Leveraging the pangenome as a reference background, SVPG accurately filters false-positive calls in germline SV detection and refines SV breakpoint coordinates, improving overall SV detection performance. Additionally, SVPG supports identification of *de novo* SVs from pangenome graphs, capturing low-frequency variants associated with rare disease or cancer-related loci, providing critical support for rare disease etiology research and personalized cancer therapeutics. Finally, novel SVs called by SVPG can be seamlessly integrated back into the pangenome framework, enabling efficient enhancement and continuous iteration of the graph structure, thereby establishing a reciprocal feedback mechanism between variant detection and graph evolution.

RESULTS

Overview of SVPG

SVPG integrates two complementary SV detection modes: pangenome-guided and pangenome graph-based SV detection (Fig. 1). In the pangenome-guided mode, SVPG first converts collected SV signals from a BAM file into signature reads and realigns these reads to the pangenome reference. By thoroughly analyzing the topological features and path transition patterns of SV signature reads in the pangenome graph, SVPG achieves high-precision SV breakpoint localization while optimizing the quality of original feature signals. In the graph-based SV mode, SVPG directly analyzes the alignment characteristics and patterns of raw read sequences within the pangenome graph structure without relying on known SV information, accurately detecting *de novo* SVs within haplotype paths of graph (see Methods for details). This dual-mode design provides SVPG with broader applicability: researchers can select the first mode for higher SV calling accuracy when high-quality pangenome references are available, or switch to the second mode for novel variant discovery when prior information is limited. Beyond the above-mentioned SV detection functions, SVPG integrates a graph augmentation pipeline, allowing researchers to rapidly call graph-based SVs from population-scale new samples and implementing graph augmentation functionality in conjunction with pangenome construction tools.

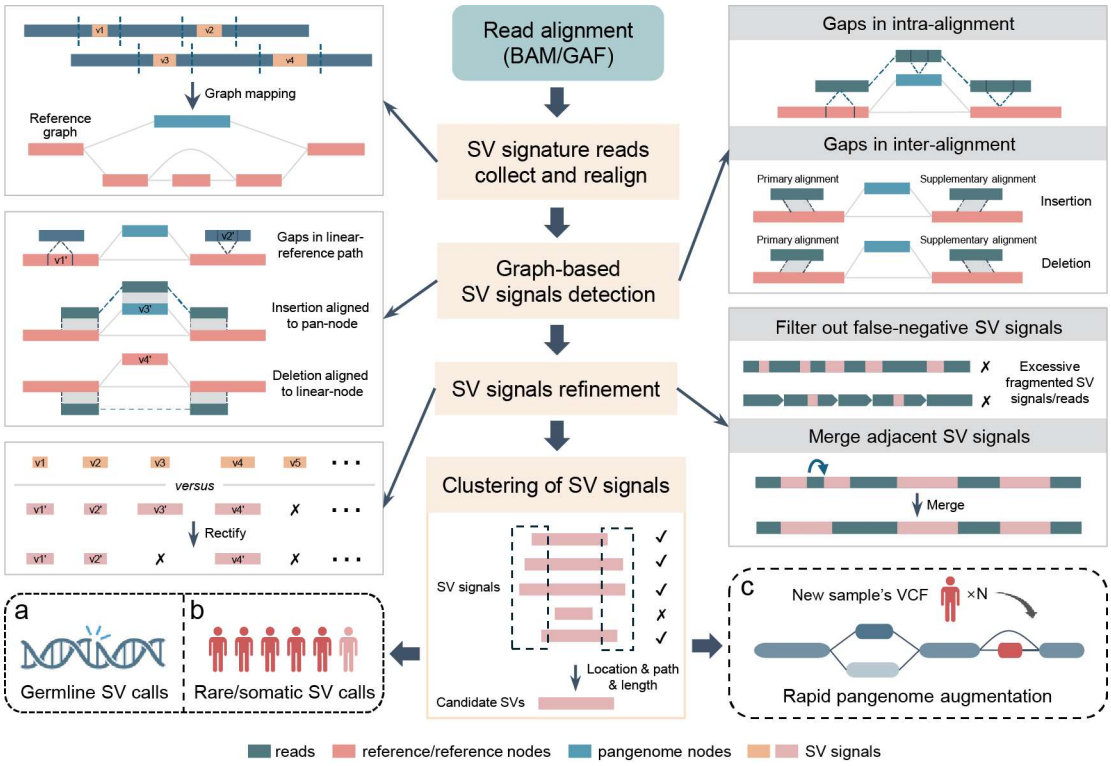

Fig. 1 | Overview of SVPG. SVPG supports two modes of SV detection, processing either BAM or GAF alignments, which correspond to pangenome-guided and pangenome graph-based SV detection, respectively. In the BAM-input mode (left), SVPG collects SV signature reads and aligns them to the pangenome reference, followed by graph-aware SV signal extraction and refinement. The GAF-input mode (right) enables direct extraction and refinement of *de novo* SV signals from sequence-graph alignments. Both modes utilize a common cluster-based refinement step, ultimately generating standard VCF output.

SVPG enables high performance SV calling on the GIAB ground truth set

We first assessed pangenome-guided mode's SV calling performance on HG002 sample's ground truth set[22], from the Genome in a Bottle (GIAB) consortium. We compared the SVPG with four leading long-read alignment-based SV callers, Sniffles2[8], cuteSV[9], SVIM[23], and DeBreak[24]. In the high-confidence SV regions, SVPG was among the top performers with F1 scores of 95.8% and 96.6% for ONT and HiFi platforms (Fig. 2a). In subsequent downsampling datasets, SVPG maintained F1 scores above 90.0% even at low-coverage conditions (ONT-10× and HiFi-5× coverage), consistently demonstrating superior detection robustness. This

exceptional SV detection capability was also reflected in genotyping accuracy, with SVPG showing the highest performer (Fig. 2b).

Next, we benchmarked performance on three representative challenging genome regions: GIAB-released HG002 tier2 regions (containing approximately 6,000 high-confidence SVs in complex or non-consensus sequences), newly defined complex graph regions based on the pangenome reference (characterized by high-frequency multi-allelic variants; see Supplementary Fig. 3 and Fig. 4 for distribution, and Methods for construction details), and clinically relevant regions defined in the Challenging Medical Relevant Genes[25] (CMRG; encompassing SVs in 273 medically significant genes). SVPG demonstrated significant performance advantage over other calling tools when analysis expanded from high-confidence to these complex regions. Particularly, SVPG achieved average F1 scores of 71.4%, 65.1%, and 88.1% across the three challenging regions using ONT dataset with multiple coverages, surpassing the others by 4–12%. For HiFi datasets, SVPG also achieved the highest F1 scores overall (Fig. 2c, see Supplementary Table 2-4 for detail). Notably, SVPG consistently maintained stable, high-precision performance under various testing conditions, facilitating the reliable discovery of SVs in complex regions. While DeBreak occasionally showed a higher precision rate in low-coverage data, this came at the cost of recall rate. In contrast, SVPG maintained balanced performance with both high-precision and recall.

Given the importance of SV detection in Mendelian disease research, we conducted Mendelian consistency analysis using two representative GIAB-released trio family datasets (Ashkenazim and Chinese Trio). SVPG achieved the lowest inconsistency levels in both families (ONT: 0.5–1.2%, HiFi: 0.7–1.1%; Fig. 2d, Supplementary Table 5). Reduction of SVs showing Mendelian inconsistency represents a crucial step in rapidly identifying *de novo* SVs, as manual screening of all inconsistent variants is typically required when searching for true *de novo* events. We further selected a subset of *de novo* SVs called by SVPG and Sniffles2, in high-confidence regions of HG002 sample for further validation using Integrative Genomics Viewer (IGV)[26] (Supplementary Note 1). In chromosomes 1–3, results revealed that two out of five *de novo* SVs called by SVPG were confirmed as high-confidence variants. In contrast, of the 13 *de novo*

SVs called by Sniffles2, 11 were either false positives or located in noisy regions with split alignments, while the remaining two genuine events were successfully identified by SVPG. These findings confirm that pangenome effectively eliminate Mendelian inconsistencies in SV calling.

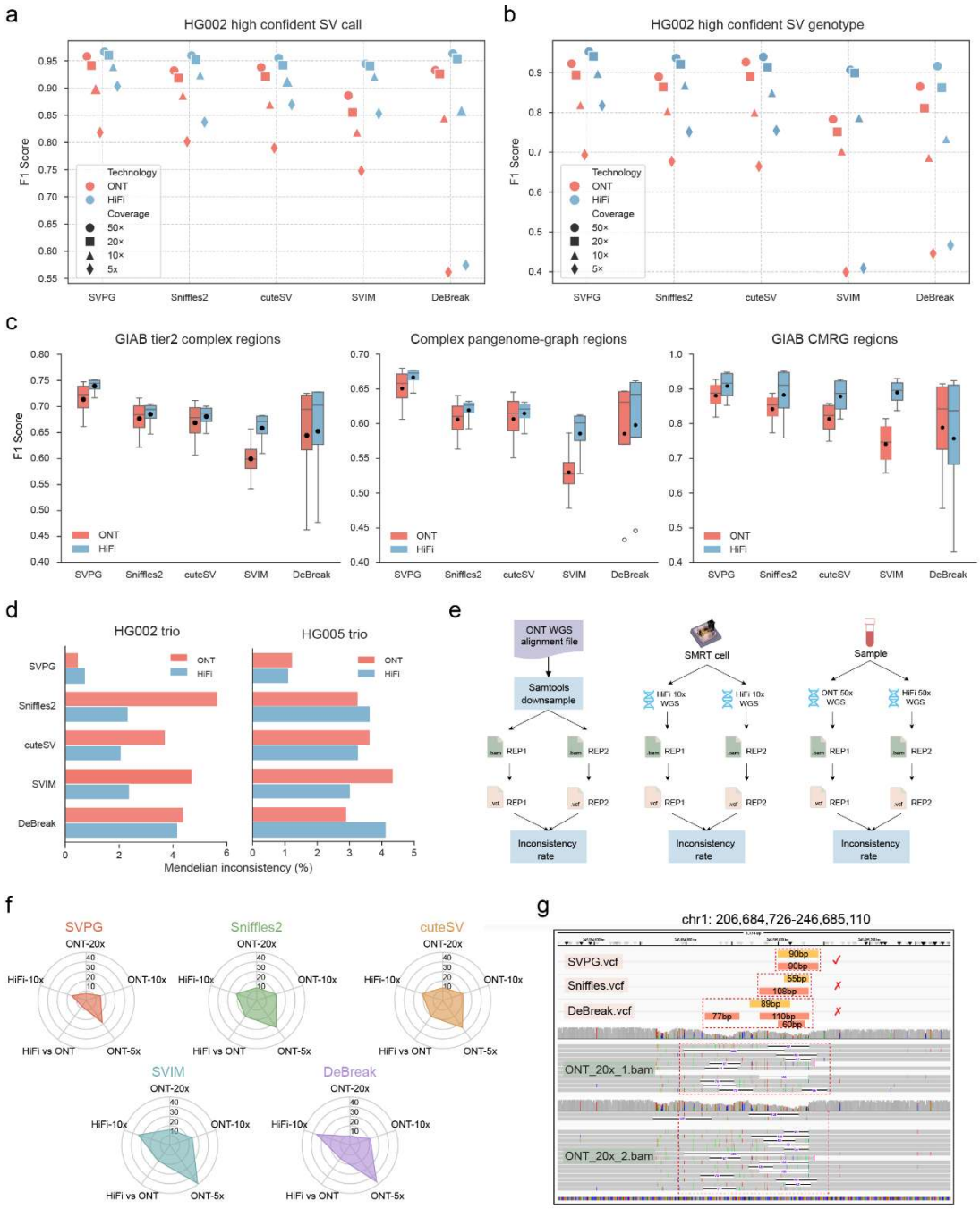

Fig. 2 | Performance assessment of SVPG in pangenome-guided SV calling. a and **b**, Comparison of SV calling and genotyping F1 score using the GIAB HG002 benchmark across

sequencing platform (ONT and HiFi) and coverage. **c**, Comparison of SV calling F1 score at multiple coverages levels (5-50×) across three complex genomic regions on HG002. **d**, Mendelian inconsistency rates across sequencing platform in HG002 and HG005 trio family. **e**, Schematic representation of three replicate-based experiments in HG002 for quantifying false positive SV calls. **f**, Replicate inconsistency rates for each SV calling tool across five experimental groups: three downsampled ONT replicates from HG002, one cross-platform comparison (HiFi vs. ONT), and one replicate group from HG005 with HiFi 10× coverage. **g**, An example of inconsistent SV calls in the ONT-20× downsampling group. In the top panel, yellow and red bars represent SVs called by SVPG, Sniffles2, and DeBreak in two downsampled replicates, respectively. SVPG achieved fully consistent calls under pangenome guidance.

False positive SV calls quantified through replicate-based experiment

Traditional SV benchmarking heavily relies on the gold standard datasets released by GIAB, which constrains evaluation comprehensiveness and introduces systematic biases. The replicate-based evaluation strategy enables the efficient quantification of false positives in SV calling. The core principle of this strategy is that genuine SVs should be consistently detected across replicates, whereas false positives arising from technical artifacts (e.g., library preparation or sequencing errors) typically appear in single samples[27-29]. Therefore, the more inconsistent events there are in replicate experiments, the higher the proportion of false positive SVs in the calls. To avoid sensitivity biases caused by uneven sequencing depth in actual repeat sequencing, we simulated replicate sample pairs with the same coverage by downsampling BAM files of the same sample, using different random seeds. We ran all calling tools on replicate sample pairs of HG002 at 20×, 10×, and 5× coverage from ONT, comparing the inconsistency of the SV sets detected. The results showed that SVPG exhibited the lowest inconsistency in all three downsampling replicate experiments (Fig. 2f, 20×: 7.1%, 10×: 15.9%, 5×: 29.9%; see Supplementary Table 6 for detail; Fig. 2g show an example), significantly outperforming other tools. As sequencing coverage decreased, the inconsistency rate of all tools increased significantly; this is consistent with the theoretical expectation that insufficient

supporting reads at low coverage leads to an increase in the number of false positives. We then validated the results using a set of 10× coverage raw HiFi sequencing data, similar results were obtained, further confirming the stability advantage of SVPG.

We further assessed the consistency of SV calls across different sequencing platforms using of HG002 HiFi and ONT data samples. Using high-accuracy HiFi data as the control, SVPG showed only an 8.8% discrepancy between platforms, substantially outperforming other tools (e.g., 17.1% of the second-best DeBreak). This exceptional cross-platform consistency of SVPG, despite similar F1 scores among tools on the same platform, highlights its ability to reduce false positives by leveraging pangenome-guided refinement. Such robustness minimizes technology-specific biases in population-scale variant analyses.

Pangenome-based rare SV calling performance assessment

Rare SVs predominantly represent recent or *de novo* structural mutations that reveal potential genomic mutation mechanisms. The 1000 Genomes Project demonstrated that 96–99% of variant alleles in the human genome are shared within populations[30], and this information has now been systematically incorporated into pangenome references. Leveraging this characteristic, we developed a graph-based SV calling mode, which established a reliable approach for sample's rare SV identification by detecting *de novo* SVs that were absent in the pangenome. To assess the approach, we curated 66,197 rare SVs of varying types and sizes from an existing database as the gold standard benchmark set[31], and generated two 20× coverage simulated datasets (ONT and HiFi) containing these representative rare variants. By using the "*bedtools jaccard*" command, we compared these SVs with the bubble regions in the pangenome reference, and found that only 2.6% of the regions overlapped, further confirming the rarity of these SVs (Methods for benchmark set construction details).

We input the simulated read alignments against the pangenome reference into SVPG's graph-based calling mode, and compared its performance with that of miniSV, which is currently the only tool supporting direct SV calling from graph alignment format. SVPG achieved F1 scores of 89.8% and 88.8% on ONT and HiFi data, respectively, surpassing that of miniSV by 8.1%

205 and 4.5%, respectively. SVPG maintained low false-positive rates while successfully recalling
206 more accurate rare SVs (Fig. 3a, Fig. 3b and Supplementary Table 7). This performance
207 advantage was consistent across different SV size ranges and SV type, with particularly notable
208 improvements in regions associated with transposable element activity, such as around 300 bp,
209 2 kb, and 6 kb (Fig. 3c). Additionally, the size distribution of rare SVs exhibited distinct
210 abundance at these intervals, implying that many of these rare SVs may be influenced by the
211 activity of transposable elements (Supplementary Fig. 5). This observation is further supported
212 by our overlap analysis between rare SVs and major classes of repeat elements (Fig. 3d). These
213 results highlight the widespread impact of repeat elements (Alu, LINE1, SVAs) in shaping
214 human genomic diversity, and high-level similarities between our SV catalogue and other
215 studies[1].

216 We further benchmarked SVPG on HG002 to analyze the performance to detect rare SVs in
217 real sample. Our evaluation was based on two key assumptions: (1) The existing pangenome
218 reference already covered the most common SVs, so *de novo* SVs called from the pangenome
219 graph are likely to represented individual-specific rare SVs; (2) An individual's rare SVs should
220 be a subset of their complete SV spectrum, with benchmark-validated SVs considered as true
221 positive. We aligned HG002 HiFi data to the pangenome reference and performed graph-based
222 SV calling using SVPG and miniSV. Overall, SVPG and miniSV recalled 580 and 409 SVs,
223 respectively, among which 188 SVPG's true positive rare SVs (miniSV: 114) were supported
224 by the GIAB benchmark. These SVs were further confirmed as genuinely rare through
225 verification against the Human Genome Structural Variation Consortium (HGSVC) dataset of
226 65 individuals (Fig. 3e). Fig. 3f shows that SVPG detects more rare true positive SVs than
227 miniSV across different SV length intervals. Fig. 3g shows an example of a rare deletion
228 detected only by SVPG, with the UCSC Genome Browser screenshot suggesting that this
229 variant may be pathogenic. For the remaining rare SVs not reported by GIAB, it is challenging
230 to definitively classify them as false positives, primarily due to the known incompleteness of
231 current benchmarks—especially in repetitive or poorly mappable regions. Many of these SVs
232 exhibit strong read-level support and are located in genomic contexts typically associated with

true rare variants, suggesting that they may represent previously uncharacterized structural changes. This interpretation is further supported by the SVPG's 82.1% precision within GIAB's high-confidence regions, where reliable ground truth enables a more accurate estimation of specificity.

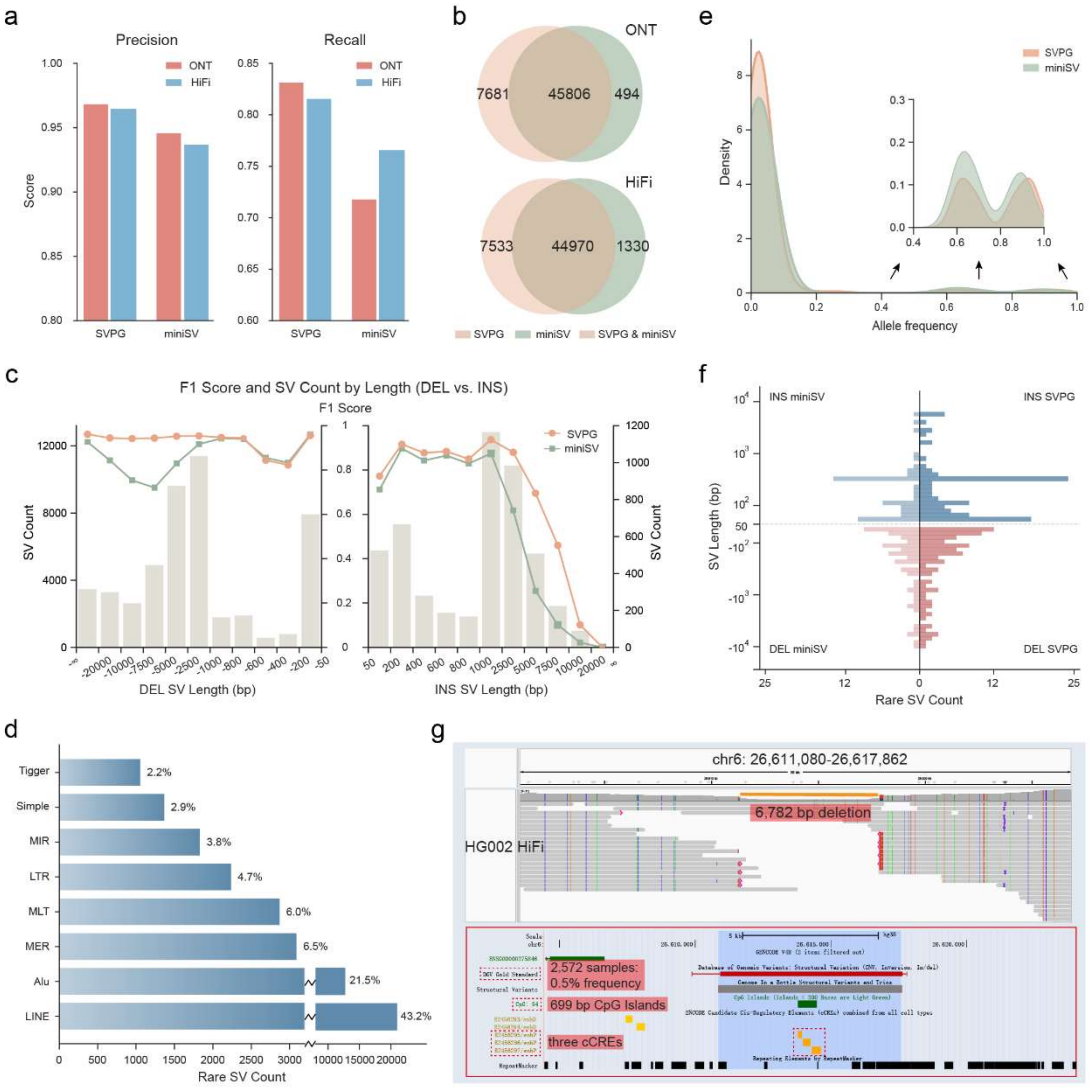

Fig. 3 | Performance evaluation of SVPG in pangenome graph-based SV calling. a, Comparison of graph-based *de novo* SV calling performance on simulated rare SV datasets. **b**, Venn diagram of rare true positive SVs detected by SVPG and miniSV on ONT and HiFi dataset. **c**, Performance comparison of different rare SV types across different SV length ranges on simulated ONT datasets. The lines indicate F1 score measure, and the bars show the number of SVs called by SVPG. **d**, Overlap analysis between SVPG rare true positive SVs from the ONT

244 dataset and common repeat family elements. **e**, Allele frequency (AF) distribution of true positive
245 SVs called by SVPG and miniSV on HG002 sample. The main panel shows kernel density
246 estimates of AF across all variants in the HGSVC dataset. The inset highlights the AF range from
247 0.4 to 1.0. **f**, Distribution of true positive rare SVs across different SV length range on HG002
248 sample. **g,** A 6,782 bp rare large deletion (chr6: 26,611,080) called by SVPG in HG002, missed
249 by miniSV. The bottom panel of UCSC Genome Browser snapshot indicates the SV supported
250 by the Database of Genomic Variants (DGV, marked in red), with a population frequency of
251 ~0.544%, confirming its rarity. The deletion overlaps a 699 bp CpG island and three candidate
252 cis-regulatory elements (cCREs, yellow), suggesting potential disruption to local regulatory
253 activity.

254 **SVPG enables enhanced somatic SV detection and benchmark refinement**

255 To evaluate the potential of pangenomes for non-germline SV detection, we applied the SVPG
256 graph-based mode into a somatic-specific SV discovery pipeline. We expected that aligning
257 reads from both tumor and adjacent normal tissues to the pangenome, rather than to the single
258 linear reference genome, may help reduce false positives caused by reference bias. We assessed
259 SVPG using recently released HiFi sequencing data from the HG008 cancer cell line and its
260 matched control[32] (see Methods for benchmark details). Results showed that SVPG accurately
261 identified the majority (38/43) of cancer-specific SVs in the GIAB benchmark set, achieving
262 the highest overall F1 score (Fig. 4a). A closer inspection of the five SVs missed by SVPG
263 revealed that four were already represented in the pangenome graph, suggesting that they are
264 likely germline SVs misannotated as somatic events (see Supplementary Note 2 for details).
265 Furthermore, compared to traditional methods relying on the linear reference genome (such as
266 Sniffles2 and Severus[33]), the pangenome-based SVPG and miniSV, both exhibited significantly
267 lower number of false positive calls, approaching the level reported by manta[34], a high-accuracy
268 short-read-based caller (Fig. 4b). These results confirm that SVPG effectively leverages
269 pangenome characteristics to achieve precise inference of somatic SVs.

270 To further evaluate the ability of SVPG to reduce potential germline SVs within existing

benchmark sets, we analyzed a widely-studied breast cancer cell line[35] (tumor HCC_{1395} and matched normal HCC_{1395}BL, respectively). We first assessed SVPG's cancer-specific SV callset (following the same calling benchmark as HG008) against HCC_{1395} consensus benchmark set (1,268 SVs identified by at least two linear reference genome-based SV callers in high-confidence regions). SVPG only identified 348 SVs consistent with the benchmark set (27.4% recall). Among the remaining 920 undetected SVs, cross-validation using bedtools revealed that 829 overlapped with node regions in the pangenome reference, suggesting that these may represent germline SVs within the consensus set (Fig. 4c and Supplementary Table 10; Figs. 4d, 4e shows two cases). In contrast, only 51 of the 348 SVs detected by SVPG showed overlap with pangenome nodes, which is significantly lower than that in the unrecalled group (Fisher's exact test, $p < 0.001$). Next, we using two SV sets from HCC_{1395} (79 indels) and COLO829[36] (35 indels), each validated by multi orthogonal experimental approaches (including PCR, BioNano, and FISH), and considered reliable references for cancer-specific SV. Within these validation sets, SVPG successfully recalled 71 and 28 events with recall rates of 89.8% and 80.0%, respectively. These results indicating of SVPG's strong tendency to capture true somatic-specific variants.

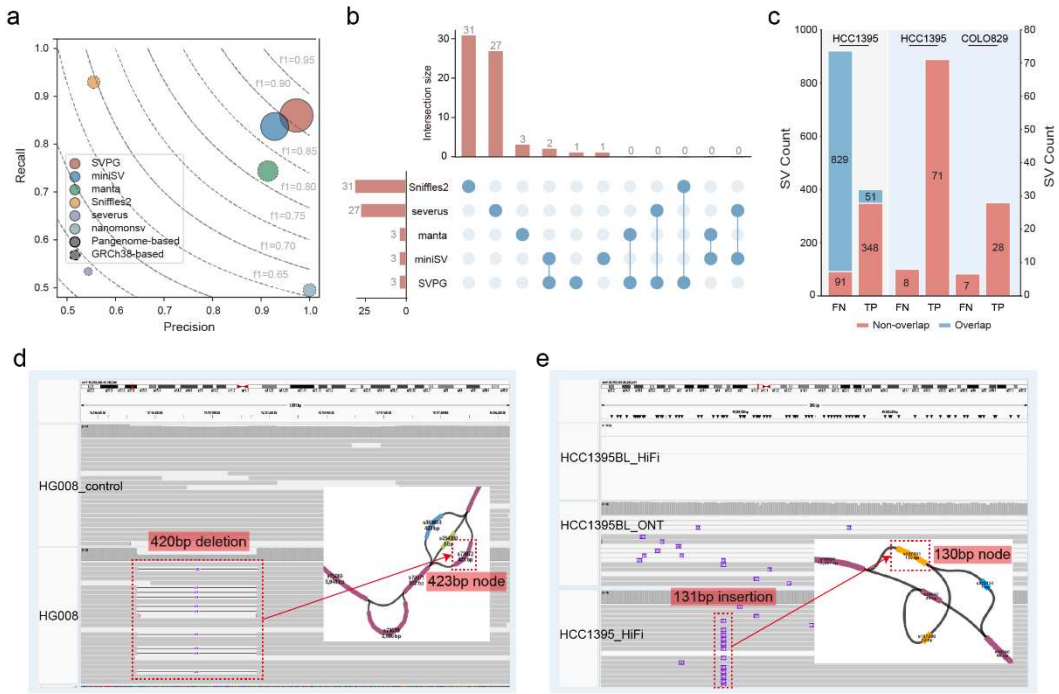

Fig. 4 | Performance evaluation of SVPG in somatic SV calling. a, Precision-Recall bubble plot of cancer-specific SVs called from HG008 sample. Solid lines represent pangenome-based methods and dashed lines represent linear reference genome-based methods. **b**, Overlap of false positive SVs detected by multiple callers in the HG008 sample. **c**, Somatic SVs detected (true positives, TP) or missed (false negatives, FN) by SVPG across benchmark sets, grouped by pangenome overlap. The left panel (grey background) summarizes SVs from the HCC_{1395} consensus benchmark set. The right panel shows results on experimentally validated benchmark set from HCC_{1395} and COLO829 (all without pangenome overlap), representing high-confidence somatic SVs. **d, e**, Two potential germline SVs identified by SVPG in HG008 and HCC_{1395} samples. **d,** IGV screenshot shows a 419 bp deletion at chr7:19,196,736 in HG008, previously reported by GIAB as cancer-specific. However, Bandage reveals that this SV is already represented in the pangenome graph. **e**, IGV screenshot displays a 131 bp insertion at chr2:89,265,288 in HCC_{1395}. HiFi and ONT reads of control sample (HCC_{1395}BL) show absent or disorganized alignments, leading multiple SV callers to misclassify it as a cancer-specific event.

Rapid pangenome graph augmentation from SVPG's graph-called SVs

Traditional pangenome augmentation typically relies on complex, time-consuming *de novo* assembly processes which require high-quality sequencing data and multiple refined assembly steps. We propose a rapid graph augmentation strategy based on *de novo* SVs identified by SVPG from graph alignments. By utilizing existing high-quality pangenome reference graphs for initial SV calling and merging, the strategy directly incorporates these variants into the original pangenome, thereby circumventing elaborate assembly procedures. Fig. 5a illustrates the key differences between the two graph augmentation strategies. We selected 20 HPRC samples' HiFi data and applied SVPG's graph augmentation mode, using the HPRC-released original pangenome reference graphs as the foundation for generating augmented versions. Analysis of population-level SVs called by SVPG revealed that these *de novo* SVs, predominantly ranging from 50–500 bp in length, existed at allele frequencies of approximately 0.1, further indicating the rarity (Fig. 5b). Subsequently, we constructed an augmented graph

316 based on *de novo* assembly using the hifiasm[37] assembler, following the standard pipeline of
317 HPRC. Given our primary focus on SVs exceeding 50bp, all graphs were constructed using
318 minigraph[38], which is optimized for capturing large-scale genomic rearrangements. Overall,
319 SVPG completed this process within half a day, while for the assembly strategy, even the initial
320 hifiasm assembly step, took up to half a week, with substantially longer timeframes when
321 including additional refined assembly procedures (Fig. 5c and Supplementary Table 12).

322 We denote the graph alignment-based augmented graph as SVPG-AUG and the assembly-based
323 augmented graph as hifiasm-AUG. Compared to the original graph, both augmentation graphs
324 exhibited a substantial increase in nodes and edges (Supplementary Table 13), indicating
325 enhanced the expressive capacity of the graph representations. Analyzing bubble regions which
326 represent variant sites within the graphs, we observed remarkable similarity between the two
327 augmented graphs. Using GRCh38 as a reference example, we found that 98% of the 92,597
328 bubbles identified in SVPG-AUG overlapped with bubbles in hifiasm-AUG (Fig. 5d). We
329 further analyzed the subset of bubble regions unique to each augmented graph with respect to
330 annotated repetitive elements. Among the 1,824 SVPG-AUG–specific bubbles, 1,322 (72.5%)
331 overlapped with known repeats, while 1,689 (76.4%) of the 2,211 hifiasm-AUG–specific
332 bubbles overlapped with repeats. Among the eight most abundant repeat families ranked by
333 overlap count (right panel of Fig. 5d), SVPG-AUG exhibited overall greater overlap lengths,
334 particularly with long interspersed elements such as LINEs and Alus. In contrast, hifiasm-AUG
335 displayed a greater number of overlapping regions, especially with shorter, high-copy elements
336 such as SIMPLE repeats. These results indicate that, despite differing methodologies, both
337 augmentation strategies yielded highly consistent variant representations, while also capturing
338 distinct repeat-associated variation.

339 To compare how pangenomes constructed from complete haplotypes capture specific
340 biologically relevant loci, we focused on the *MUC6* gene region, a locus known for its extensive
341 polymorphism and strong clinical relevance[39] (see UniProt entry:
342 https://www.uniprot.org/uniprotkb/Q6W4X9/entry). We extracted the subgraph corresponding
343 to *MUC6* regions (chr11:1,012,823-1,036,718), allowing us to directly inspect how structural

diversity is represented across different graph. As shown in Fig. 5e (PanGraphViewer[40] for graph visualization), SVPG-AUG (bottom) subdivides an original segment into five distinct nodes, capturing sample-specific structural rearrangements contributed by HG00140 and HG00323 samples. In contrast, hifiasm-AUG maintains a topology similar to the original graph (Supplementary Fig.8), indicating a more conservative representation of variation in this region. As another case study, we examined 881 genomic regions in the HG00097 sample where hifiasm failed to assemble long-read sequences (all exceeding the 15 kbp average HiFi read length). Within these regions, SVPG identified 25 *de novo* SVs. Fig. 5f presents an example where an SVPG-called SV was successfully incorporated to augment the graph: a 143 bp insertion called by SVPG at the assembly-failed region in the HG00097 sample and encoded in the augmented graph, by decomposing the normal path to create a corresponding bubble structure (s371207). In conclusion, these findings strongly demonstrate that SVPG can effectively augment pangenome structures in assembly-challenging regions, providing more comprehensive genomic characterization for SV analysis.

Finally, we aligned HG002 HiFi data to the pangenome graphs to assess the impact of augmented graphs on downstream applications. Minigraph alignment showed that both augmented graphs improved mapping over the original graph. SVPG-AUG yielded 2,551 more alignment records and 68 Mbp of additional aligned bases, with slightly higher than hifiasm-AUG (Fig. 5g, Supplementary Table 14). Further, we substituted the original graph with augmented graphs to examine their influence on SV calling under the SVPG pangenome-guided mode. Results indicated that the SVPG's calling performance remained largely consistent across both augmented graphs. In the CMRG regions, SVPG-AUG exhibited modest improvements (Supplementary Table 15). These findings indicate that current pangenome references already capture substantial SV information, and augmented graphs have yet to show marked improvements in common germline SV calling within current benchmarks. However, with advancing technologies and expanding datasets, optimized pangenomes may offer greater benefits, particularly in complex variant regions or diverse population analyses.

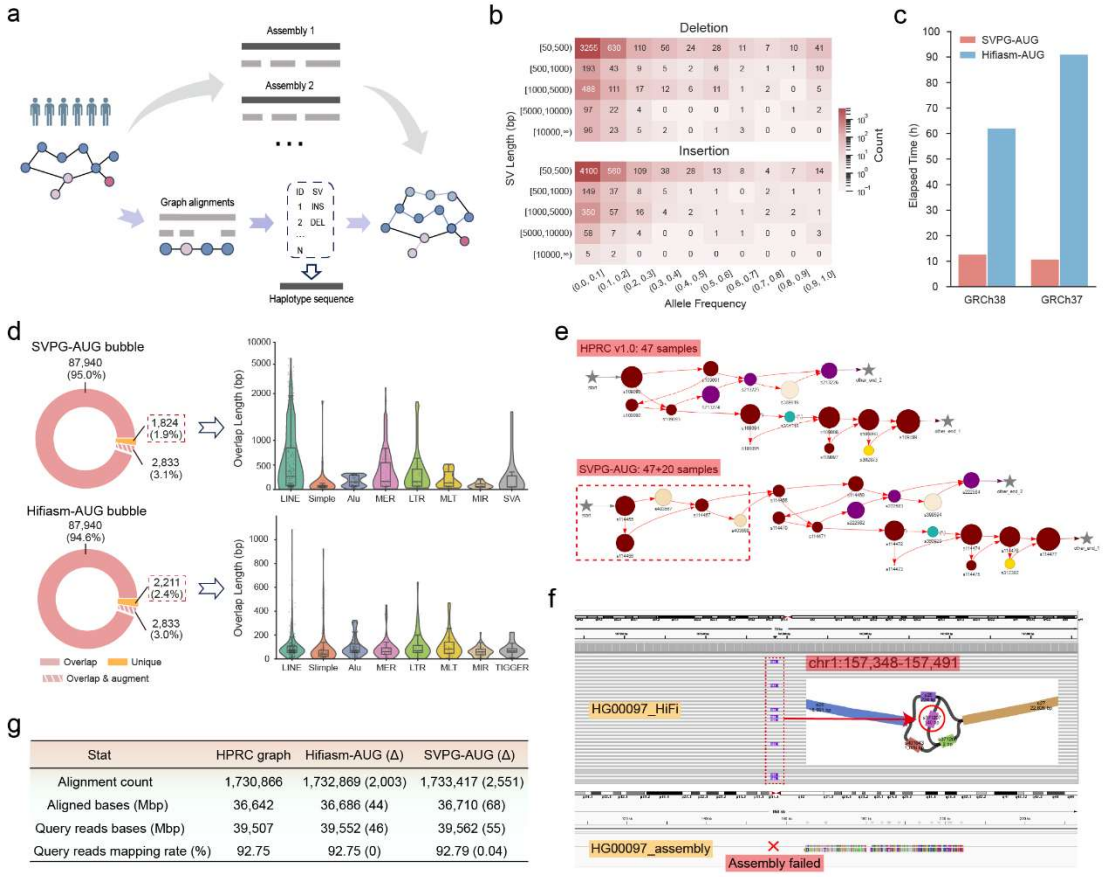

Stat	HPRC graph	Hifiasm-AUG (Δ)	SVPG-AUG (Δ)
Alignment count	1,730,866	1,732,869 (2,003)	1,733,417 (2,551)
Aligned bases (Mbp)	36,642	36,686 (44)	36,710 (68)
Query reads bases (Mbp)	39,507	39,552 (46)	39,562 (55)
Query reads mapping rate (%)	92.75	92.75 (0)	92.79 (0.04)

Fig. 5 | SVPG pangenome graph augmentation results. **a**, Comparison of two approaches to pangenome graph augmentation. The upper grey arrows depict iterative graph augmentation through *de novo* assemblies of new samples (hifiasm-AUG). The lower path shows augmentation through integration of population-scale variant calls from graph alignments (SVPG-AUG). **b,** Distribution of SVs called by SVPG across 20 HPRC samples by SV length and allele frequency. **c**, Comparison of computational time required for constructing SVPG-AUG and hifiasm-AUG. **d**, Composition of bubble regions in GRCh38-based SVPG-AUG and hifiasm-AUG. 'Overlap' indicates non-augmented bubbles that are shared between the two augmented graphs (original graph bubbles); 'Overlap & augment' represents newly added bubbles compared to the original graph; 'Unique' denotes bubbles exclusively found in one augmented graph and not found in the other. The violin plot on the right shows the distribution of overlaps between unique bubbles from SVPG-AUG and hifiasm-AUG and repetitive elements. Only the top eight repeat families with the highest overlap counts are shown. For

385 SVPG-AUG, due to the wide range of overlap lengths, values >1,000 bp are log-transformed.
386 **e,** Local graph topology at the *MUC6* locus. From top to bottom: the original graph (17 nodes),
387 and SVPG-AUG (22 nodes). Additional nodes introduced by SVPG-AUG are highlighted in
388 red box. **f**, A SVPG-AUG-specific node example. The upper IGV panel shows a 143 bp
389 insertion at chr1:157,348 in HG00097 sample, called by SVPG and successfully integrated into
390 the graph. The lower IGV panel indicates that hifiasm failed to assemble this region. **g,**
391 Summary of alignment metrics obtained by mapping HG002 HiFi reads to the HPRC GRCh38-
392 based pangenome graph and its two corresponding augmented versions. Δ denotes the increase
393 compared to the original graph.

394 **Discussion**

395 This study introduces SVPG, a method to incorporate pangenome information into SV detection
396 of long-read sequencing. Our results demonstrate the performance of SVPG across sequencing
397 platforms and depths compared to existing tools, with advantages further validated through
398 complex genomic region analyses and Mendelian inconsistency tests. A highlight of SVPG is
399 its computational reproducibility and robustness, as demonstrated by unbiased replicate
400 experiments for false-positive quantification, where SVPG exhibited significantly higher
401 consistency and cross-platform stability compared to other tools. These findings not only
402 validate the critical importance of pangenome information in SV detection but also provide a
403 new technical paradigm for future developments in this field.

404 Furthermore, the SVPG graph-based SV calling mode enables *de novo* SV detection from
405 pangenome graph. This offers a novel perspective on rare SV discovery, which traditionally
406 relies on large-scale population sequencing data analysis—an approach that is both resource
407 intensive and prone to missing individual-specific rare variants, particularly without adequate
408 genetic background references. SVPG graph-based detection leverages population genetic
409 variation information embedded in pangenomes to achieve accurate rare SV detection at the
410 single-sample level with high sensitivity, eliminating the need for population-scale data support.
411 This capability has significant implications for elucidating disease-associated variants and

individual-specific phenotypic mechanisms.

Notably, our tool demonstrates that pangenome significantly enhances the detection of somatic SVs, the specialized and distinct class of rare SVs. By introducing a pangenome background to effectively filter out the majority of germline SVs, SVPG outperforms linear reference-based methods with much higher precision. Building on this advantage, SVPG more precisely identified cancer-specific variants through the construction of personalized or population-specific pangenome references from matched normal tissues or cell lines. Further analysis revealed that some false negative SVs unreported by SVPG are actually visible in the germline-derived pangenome, suggesting that current published cancer SV benchmark sets may contain non-genuine cancer-driving somatic mutations. This finding emphasizes that pangenome background is an essential factor when constructing cancer-specific SV benchmark sets. In future research, SVPG may serve as an auxiliary screening tool in cancer SV consensus set construction for confidence-level stratification and low-quality variant identification. For instance, SVs undetected by SVPG and lacking external evidence support may be labeled as "low-confidence somatic SVs" or excluded altogether, thereby reducing potential interference risks in subsequent biological validation and functional studies.

Our exploration of SVPG application in pangenome graph augmentation yielded promising results. Using graph SVs called from 20 human samples, we implemented a graph alignment-based augmentation pipeline. The results demonstrate that SVPG-called graph SVs can effectively integrate into existing pangenomes, producing augmented graphs highly concordant with those derived from traditional *de novo* assembly-based approaches. By circumventing complex assembly processes, this graph alignment-based strategy reduced the time required for graph augmentation nearly 10-fold across 20 samples. This efficiency is expected to increase further with larger sample sizes, offering an efficient solution for large-scale, rapid pangenome graph iteration.

Though this study represents an initial attempt at leveraging pangenomes for SV detection, it still faces several unresolved challenges. First, precise SV detection and reliable assessment in

complex genomic regions remain challenging. SVPG performance heavily depends on graph alignment accuracy, where mapping quality of minigraph in certain complex regions requires improvement, while GraphAligner[41] computational inefficiency precludes large-scale graph SV calling. Besides introducing more specific heuristics for complex regions, improving graph alignment algorithms remains crucial for advancing graph-based SV detection. Second, while alignment-based graph augmentation approaches offer efficient and cost-effective solutions, they rely on an intricate pipeline of multiple tools, including graph alignment, variant calling and merging, and graph construction. This multi-tool dependency introduces compound error sources that are particularly pronounced in multi-allelic regions, where sequence similarities and structural complexities can cascade through each analytical step. In the future, incorporating local assembly may may be beneficial for improving sequence accuracy.

As initiatives like HPRC progress and reference graphs continue to evolve, pangenome references are expected to rapidly expand to thousands of haplotypes in the coming years. In this context, the high accuracy and versatility of SVPG position it advantageously for both SV detection and graph augmentation. We anticipate that pangenome-based SV detection methods like SVPG will play an increasingly crucial role in whole-genome analysis pipelines.

Methods

SVPG methodology

SV signature reads collection and realignment

In the pangenome-guided detection mode, SVPG takes linear reference genome alignment result as the input and extracts SV signatures through two heuristic rules, according to the signal source type: (1) gap sequences in the CIGAR string of primary alignments exceeding predefined thresholds, indicating potential insertions or deletions, and (2) abnormal distances between primary and supplementary alignments from split-read mapping, with sequence lengths exceeding predefined thresholds, usually indicating more complex or larger SVs.

Each detected SV signal is instantiated as an independent object with key attributes: breakpoint

465 coordinates in both reference genome and reads, complete read sequence, read name, and signal
466 source type. SVPG then scans each SV signal object to generate SV signature reads based on
467 their attributes. In the standard pipeline, SVPG extracts an additional 2,000 bp window
468 sequence on both sides of the breakpoints of the SV signal as alignment anchors. For signals
469 from split alignments, the complete original read sequences are used directly. Notably, when
470 SV breakpoints are less than 2,000 bp from read ends, SVPG supplements missing sequences
471 from the reference genome based on the SV signal's reference breakpoint position, to ensure
472 sequence window completeness. These flanking sequences are concatenated with SV signal
473 sequences to form complete signature read sequences, with key SV signal attributes recorded
474 in the read description line, for subsequent refinement steps.

475 SVPG employs minigraph for rapid realignment of SV signature reads to the pangenome
476 reference graph. Parameters are configured according to sequencing data types: "*-x asm*" for
477 HiFi data and "*-x lr*" for ONT data. The "*-vc*" parameter enables output of unstable sequence
478 coordinates to support standard GFA graph format.

479 **Graph-aware SV signal detection and refinement**

480 Unlike BAM files using linear reference coordinates, GAF data structure describes sequence-
481 to-graph alignment information through graph paths and path coordinates. Graph paths
482 comprise ordered nodes and edges, with each node's start and end uniquely corresponding to
483 linear reference coordinates. SVPG first converts the pangenome graph structure into a
484 dictionary for efficient node querying and graph traversal, with the node name as keys and their
485 properties (sequence length, coordinate information, and topological relationships) as values.

486 Graph-aware SV signal detection handles two scenarios: (1) Alignment paths containing only
487 linear reference nodes. Here, path discontinuities typically indicate deletions. SVPG accesses
488 the graph dictionary by the missing node names to obtain node coordinates and spans, which
489 accurately represent the SV breakpoints. Additionally, gaps in path CIGAR strings further
490 localize SV breakpoints based on path-start nodes and alignment-start coordinates. (2)
491 Alignment paths including non-reference haplotype nodes. SVPG identifies insertions based on

haplotype nodes, with variant spans equal to the total span of all haplotype nodes between linear reference nodes. For CIGAR string gaps, processing depends on gap location. Gaps in linear reference node paths are preserved; gaps in haplotype node paths adjust the insertion span represented by that haplotype node. Specifically, insertion-induced gaps increase the original insertion span by the gap length, while deletion-induced gaps decrease it. Finally, for complex paths containing both haplotype and discontinuous nodes, SVPG preserves deletion signals represented by missing nodes, and subtracting haplotype node length from signal span.

The complex topology of pangenome graphs is more prone to alignment artifacts, particularly in highly variable or repetitive regions. To mitigate these effects, SVPG implements stringent signal refinement: all graph-called SV signals within the same signature read are compared against the original SV signature signal for filtering. Specifically, SVPG selects graph-called SVs with breakpoints closest to the raw SV signal. If the graph SV signal span does not meet consistency principles with the raw signal span, all graph SV signals from that signature read are filtered out. The consistency principle determines the reliability of an SV signal based on the span of the called SV ($span_{graph}$) and raw SV signal ($span_{raw}$); if $\frac{min(spa_{graph}, span_{raw})}{max(span_{graph}, span_{raw})} > 0.5$, the SV signal is considered highly reliable.

Clustering of SV signal

SVPG employs a two-stage clustering strategy to transform scattered graph SV signals into candidate SVs. The first stage performs coarse-grained clustering based on spatial similarity, grouping SV signals of the same type into initial clusters, if their breakpoint distances are within a predefined threshold (default 1,000 bp). This spatial proximity-based clustering broadly captures multiple signals originating from the same SV event.

The second stage focuses on SV signal feature similarity analysis, refining the initial clusters through three feature dimensions: variant span, breakpoint coordinates, and graph path. Span similarity undergoes difference-based normalization, while breakpoint coordinate similarity is normalized using span and parameter σ, where σ is determined by both local cluster SV signal

abundance (*localN*) and global SV signal abundance (*globalN*): $\sigma = \frac{|localN - glob\quad|}{max(localN, globalN)} + globalN$. Graph path similarity employs Jaccard distance with a penalty μ (default 0.05). The overall similarity between any two SV signals is expressed as: $S = \frac{1}{max(span_1, span_2)}\left(|span_1 - span_2| + \frac{|loc_1 - loc_2|}{\sigma}\right) + \mu \times \left(1 - \frac{path_1 \cap path_2}{path_1 \cup path_2}\right)$. Based on multi-dimensional feature similarity analysis, initial clusters undergo hierarchical clustering (default threshold 0.3) to form highly homogeneous subclusters, each representing potential SV alleles in local genomic regions.

SV call and genotyping

Before finalizing candidate SVs, SVPG implements a quality control strategy based on minimum supported reads and alignment path consistency. For each SV cluster, variants sharing identical graph traversal paths are subject to a relaxed read support threshold, effectively recovering high-quality SV signals that may otherwise be missed due to insufficient sequencing depth. This pangenome-based alignment path consistency filtering mechanism effectively balances the sensitivity and specificity of detection.

Clusters passing quality control proceed to final SV calling and genotyping. SVPG uses the median of all SV signal breakpoint coordinates within a cluster as the final candidate SV breakpoint coordinates. Additionally, the SVPG genotyping module assigns optimal genotypes (0/0, 0/1, and 1/1) to each candidate SV through maximum likelihood estimation based on sequence coverage statistics in variant flanking regions.

Graph-aware *de novo* SV signal detection and refinement

SVPG graph SV detection mode processes GAF format that graphs alignments, converting gap information from each alignment path's CIGAR string into corresponding SV signals. Besides internal graph alignment information, SVPG encodes SV signals from external graph alignments. Given the lack of explicit supplementary alignment markers in the GAF format compared to BAM format, SVPG sorts multiple alignment records from the same read by genomic position, designating the upstream alignment as primary, and determines SV

544 breakpoint coordinates through primary-supplementary alignment relationships.

545 Subsequently, SVPG implements post-processing steps to enhance SV signal quality, including:
546 (1) filtering SV signals from reads exceeding thresholds for fragmented SV signals or split
547 operations during alignment; (2) refining SV breakpoints in repetitive regions by identifying
548 locally redundant signals within same genomic windows, and removing inconsistent or spurious
549 SV signals arising from ambiguous alignments in repetitive contexts; (3) merging same-type
550 SV signals' heterogeneous breakpoints from the same alignments record when their distances
551 fall below a preset threshold (default 500 bp). All SV breakpoints are normalized to a unified
552 coordinate system based on the reference genome, by adjusting for the orientation of their
553 originating graph nodes. Finally, collected SV signals undergo clustering and calling steps
554 identical to the pangenome-guided SV detection mode, with results output in VCF format.

555 **Graph augment module**

556 SVPG integrates multiple tools to achieve rapid graph augment. Users can provide input
557 through either an organized workspace containing sample sequencing files or a comprehensive
558 file list documenting paths to all sequencing data. For each sample, the workflow begins with
559 minigraph alignment of raw sequencing data to the original pangenome, followed by
560 implementation of the SVPG graph-based SV calling mode to call *de no* SVs. Population-level
561 SVs undergo systematic integration through a multi-step process. First, multi-sample VCFs are
562 merged using the "*bcftools merge*", and redundant variants are eliminated through "*Truvari*
563 *collapse*". Subsequently, these SVs are incorporated into the linear reference genome (the initial
564 haplotype used to construct the original pangenome) using "*bcftools consensus*", generating a
565 haplotype sequence. Before augmentation, uncertain nucleotides ("N") in the sequence are
566 removed to improve alignment efficiency. The resulting haplotype sequence, serving as a carrier
567 for all *de novo* SVs, is ultimately integrated into the original pangenome graph via "*minigraph*
568 *-cxggs*", completing the graph augment process.

569 **Benchmarking methodology**

570 **Benchmarking SV callers on GIAB high-confidence and complex regions**

571 Based on the latest GIAB release, we downloaded HG002 sample raw sequencing reads (HiFi
572 and ONT) alignment data based on the GRCh37 reference genome, and applied SVPG,
573 Sniffles2 (v2.3.3), cuteSV (v2.1.1), SVIM (v1.4.1), and DeBreak (v1.2) to perform SV calling.
574 SVPG adopts the GRCh37-91c.r559 pangenome reference release by HPRC as "*-gfa*" parameter
575 input. Except for Sniffles2 and DeBreak automatically calculating supporting reads, other tools
576 used the same supporting read threshold for low-quality call filtering (Supplementary Note 3 for
577 command lines details).

578 According to HG002 sample's gold standard sets (including HG002_SVs_Tier1_v0.6,
579 HG002_GRCh37_CMRG_SV_v1.00), all SV calling results were uniformly assessed using
580 Truvari[42] (v5.2), with the "*--includebed*" parameter specifying high-confidence regions and
581 complex genomic regions.

582 Complex graph regions were created using custom scripts. The script traverses the pangenome
583 reference graph along linear reference genome coordinates with a 5,000 bp window size,
584 counting the number of nodes in each window. If the node count >3, the window-covered region
585 is defined as a complex graph region.

586 **Mendelian inconsistency analysis**

587 We selected two family datasets, Ashkenazim and Chinese family trio datasets for Mendelian
588 inconsistency analysis. Ashkenazim trio sample data directly used GIAB-released HiFi
589 alignment data. Chinese trio samples lacked GIAB-provided HiFi platform alignment results;
590 therefore, we used minimap2 (parameters: "*-ax map-hifi*") to align raw HiFi reads to the
591 GRCh37 reference genome. In the evaluation, we selected all SV records >50 bp from the VCF
592 file of each family for consistency verification. Specifically, for the same SV record within the
593 family (with breakpoint distance <1,000 bp), we extracted genotype trios (offspring, father, and
594 mother) and verified their consistency according to Mendelian inheritance rules. For example,
595 when the genotypes of both parents are 0/0, the genotype of the offspring must be 0/0; when
596 one parent is 0/0 and the other is 1/1, the genotype of the offspring must be 0/1. Finally, we
597 calculated the Mendelian inconsistency rate by dividing the number of inconsistent records by

598 the total number of records.

599 **Benchmarking the performance of SV caller using replicates**

600 We assessed the inconsistency of replicate experiments using multiple datasets from HG002
601 and HG005 samples. For the 48× ONT alignment data of HG002, we performed downsampling
602 using "*samtools view*" with default and 99 random seeds to construct paired datasets at 20×,
603 10×, and 5× coverage. For the HG005 sample, we selected two independent 10× coverage HiFi
604 sequencing datasets and aligned the raw reads to the GRCh37 reference genome using
605 minimap2. In the reproducibility assessment, we employed scripts similar to those used in
606 Mendelian consistency analysis, extracting genotypes from control and case groups for each
607 identical SV record and checking their concordance. The inconsistency rate was calculated by
608 dividing the number of discordant records by the total number of records. Additionally, we
609 incorporated SURVIVOR[43], a third-party SV merging tool, to calculate Jaccard similarity for
610 further validation of our assessment accuracy. Specifically, we merged VCF files from two
611 replicate experiments using parameters "*1000 2 1 1 0 50*" and "*1000 1 1 1 0 50*", then computed
612 Jaccard similarity (A/B) based on the intersection (A) and union (B) of SV records from both
613 files.

614 **Rare SV detection benchmarking in simulated data**

615 To assess rare SV detection performance, we designed a pipeline to extract 66,197 rare SVs[31]
616 from the National Human Genome Research Institute (NHGRI) repository to simulate a "super-
617 variant". Initially, we filtered 95,000 rare indels (duplications were treated as insertions) from
618 the original SV callset using two criteria: "NSAMP" and "NFAM" = 1, identifying SVs unique
619 to single individuals or families among 14,623 individuals. Subsequently, we removed
620 overlapping SVs, randomly added base sequences of corresponding variant lengths to insertion
621 <ALT> fields, and for deletions, retrieved base sequences from reference genome breakpoint
622 positions for the <REF> fields. Following this preprocessing, we established 66,197
623 independent rare SVs as our validation benchmark. We then integrated these SVs into the
624 GRCh38 reference genome using "*bcftools consensus*" to construct the "super-variant". Based

625 on this variant reference sequence, we simulated 20× coverage ONT and HiFi raw sequencing
626 reads using PBSIM3[44], aligned them to the pangenome reference (GRCh38-90c.r518 version)
627 using minigraph, generating graph alignment results. Finally, these alignments were input to
628 SVPG and miniSV for SV calling; evaluation result from the Truvari summary output files.

629 **Somatic SV detection benchmarking in HG008 sample**

630 We obtained high-coverage HiFi sequencing data for HG008 and its matched control from
631 GIAB and aligned them to GRCh38 reference pangenome using minigraph. The resulting graph
632 alignment files underwent independent SV calling through SVPG. Subsequently, we identified
633 cancer-specific SVs through SV subtraction via SURVIVOR, which merged and filtered VCF
634 files according to defined overlap criteria: SVs in the cancer sample were classified as cancer-
635 specific if their breakpoint did not overlap with that of a normal sample SV within a 1,000 bp
636 window; otherwise, it was considered non-specific. For miniSV, we followed the "tumor-
637 normal pairs" mode as documented on GitHub to identify specific SVs. For Sniffles2, we
638 employed the same SV subtraction procedure as SVPG, but using GRCh38 linear reference
639 genome's alignments as input. Manta[34], severus[33] and nanomonsv[45] directly generated tumor-
640 specific SVs from paired tumor-normal alignment files. Performance evaluation employed
641 Truvari benchmarking as recommended by the GIAB.

642 **Graph augmentation benchmarking in 20 HPRC samples**

643 HPRC has released raw sequencing data for over 300 samples. From this dataset, we selected
644 20 samples that were not included in the draft pangenome reference and input them into the
645 SVPG graph augment mode. For *de novo* assembly-based graph augment, an automated
646 pipeline was employed: hifiasm was used to assemble haplotype-resolved sequences for the 20
647 samples, which were then iteratively integrated into the original pangenome using minigraph.
648 Basic statistics for graphs were compiled using "*gfatools stat*", with bubble overlap counts
649 determined using "*bedtools intersect*" (with "*gfatools bubble*" converting graph bubbles into
650 BED format). Additionally, HG002 HiFi sequencing data was aligned to both original and
651 augmented graphs, and alignment statistics were generated using custom scripts.

References

1. Sudmant, P.H. et al. An integrated map of structural variation in 2,504 human genomes. *Nature* **526**, 75-81 (2015).
2. Kidd, J.M. et al. A human genome structural variation sequencing resource reveals insights into mutational mechanisms. *Cell* **143**, 837-847 (2010).
3. Korbel, J.O. et al. Paired-end mapping reveals extensive structural variation in the human genome. *Science* **318**, 420-426 (2007).
4. Cortes-Ciriano, I. et al. Author Correction: Comprehensive analysis of chromothripsis in 2,658 human cancers using whole-genome sequencing. *Nat Genet* **55**, 1076 (2023).
5. Stankiewicz, P. & Lupski, J.R. Structural variation in the human genome and its role in disease. *Annu Rev Med* **61**, 437-455 (2010).
6. Lupski, J.R. Structural variation mutagenesis of the human genome: Impact on disease and evolution. *Environ Mol Mutagen* **56**, 419-436 (2015).
7. Chiang, C. et al. The impact of structural variation on human gene expression. *Nat Genet* **49**, 692-699 (2017).
8. Smolka, M. et al. Detection of mosaic and population-level structural variants with Sniffles2. *Nat Biotechnol* **42**, 1571-1580 (2024).
9. Jiang, T. et al. Long-read-based human genomic structural variation detection with cuteSV. *Genome Biol* **21**, 189 (2020).
10. Ballouz, S., Dobin, A. & Gillis, J.A. Is it time to change the reference genome? *Genome Biol* **20**, 159 (2019).
11. Matthews, C.A., Watson-Haigh, N.S., Burton, R.A. & Sheppard, A.E. A gentle introduction to pangenomics. *Brief Bioinform* **25** (2024).
12. Siren, J. et al. Pangenomics enables genotyping of known structural variants in 5202 diverse genomes. *Science* **374**, abg8871 (2021).
13. Wang, T. et al. The Human Pangenome Project: a global resource to map genomic diversity. *Nature* **604**, 437-446 (2022).
14. Liao, W.W. et al. A draft human pangenome reference. *Nature* **617**, 312-324 (2023).
15. Taylor, D.J. et al. Beyond the Human Genome Project: The Age of Complete Human Genome Sequences and Pangenome References. *Annu Rev Genomics Hum Genet* **25**, 77-104 (2024).
16. Li, G., Jiang, T., Li, J. & Wang, Y. PanSVR: Pan-Genome Augmented Short Read Realignment for Sensitive Detection of Structural Variations. *Front Genet* **12**, 731515 (2021).
17. Eggertsson, H.P. et al. GraphTyper2 enables population-scale genotyping of structural variation using pangenome graphs. *Nat Commun* **10**, 5402 (2019).
18. Hickey, G. et al. Genotyping structural variants in pangenome graphs using the vg toolkit. *Genome Biol* **21**, 35 (2020).
19. Ebler, J. et al. Pangenome-based genome inference allows efficient and accurate genotyping across a wide spectrum of variant classes. *Nat Genet* **54**, 518-525 (2022).
20. Soylev, A. et al. SVarp: pangenome-based structural variant discovery. *bioRxiv*, 2024.2002.

2018.580171 (2024).
21. Li, H. & Qin, Q. miniSV: Lightweight mosaic/somatic SV caller for long reads. (2023).
22. Zook, J.M. et al. A robust benchmark for detection of germline large deletions and insertions. *Nat Biotechnol* **38**, 1347-1355 (2020).
23. Heller, D. & Vingron, M. SVIM: structural variant identification using mapped long reads. *Bioinformatics* **35**, 2907-2915 (2019).
24. Chen, Y. et al. Deciphering the exact breakpoints of structural variations using long sequencing reads with DeBreak. *Nat Commun* **14**, 283 (2023).
25. Wagner, J. et al. Curated variation benchmarks for challenging medically relevant autosomal genes. *Nat Biotechnol* **40**, 672-680 (2022).
26. Robinson, J.T., Thorvaldsdottir, H., Wenger, A.M., Zehir, A. & Mesirov, J.P. Variant Review with the Integrative Genomics Viewer. *Cancer Res* **77**, e31-e34 (2017).
27. Fang, L.T. et al. Establishing community reference samples, data and call sets for benchmarking cancer mutation detection using whole-genome sequencing. *Nat Biotechnol* **39**, 1151-1160 (2021).
28. Griffith, M. et al. Optimizing cancer genome sequencing and analysis. *Cell Syst* **1**, 210-223 (2015).
29. Elrick, H. et al. SAVANA: a computational method to characterize structural variation in human cancer genomes using nanopore sequencing. *Cancer Res* **83** (2023).
30. Genomes Project, C. et al. A global reference for human genetic variation. *Nature* **526**, 68-74 (2015).
31. Abel, H.J. et al. Mapping and characterization of structural variation in 17,795 human genomes. *Nature* **583**, 83-89 (2020).
32. McDaniel, J.H. et al. Development and extensive sequencing of a broadly-consented Genome in a Bottle matched tumor-normal pair. *bioRxiv* (2024).
33. Keskus, A. et al. Severus: accurate detection and characterization of somatic structural variation in tumor genomes using long reads. *medRxiv* (2024).
34. Chen, X. et al. Manta: rapid detection of structural variants and indels for germline and cancer sequencing applications. *Bioinformatics* **32**, 1220-1222 (2016).
35. Talsania, K. et al. Structural variant analysis of a cancer reference cell line sample using multiple sequencing technologies. *Genome Biol* **23**, 255 (2022).
36. Espejo Valle-Inclan, J. et al. A multi-platform reference for somatic structural variation detection. *Cell Genom* **2**, 100139 (2022).
37. Cheng, H., Concepcion, G.T., Feng, X., Zhang, H. & Li, H. Haplotype-resolved de novo assembly using phased assembly graphs with hifiasm. *Nat Methods* **18**, 170-175 (2021).
38. Li, H., Feng, X. & Chu, C. The design and construction of reference pangenome graphs with minigraph. *Genome Biol* **21**, 265 (2020).
39. Morales, J. et al. A joint NCBI and EMBL-EBI transcript set for clinical genomics and research. *Nature* **604**, 310-315 (2022).
40. Yuan, Y., Ma, R.K.-K. & Chan, T.-F. PanGraphViewer: a versatile tool to visualize pangenome graphs. *bioRxiv*, 2023.2003. 2030.534931 (2023).
41. Rautiainen, M. & Marschall, T. GraphAligner: rapid and versatile sequence-to-graph alignment. *Genome Biol* **21**, 253 (2020).

42. English, A.C., Menon, V.K., Gibbs, R.A., Metcalf, G.A. & Sedlazeck, F.J. Truvari: refined structural variant comparison preserves allelic diversity. *Genome Biol* **23**, 271 (2022).
43. Jeffares, D.C. et al. Transient structural variations have strong effects on quantitative traits and reproductive isolation in fission yeast. *Nat Commun* **8**, 14061 (2017).
44. Ono, Y., Hamada, M. & Asai, K. PBSIM3: a simulator for all types of PacBio and ONT long reads. *NAR Genom Bioinform* **4**, lqac092 (2022).
45. Shiraishi, Y. et al. Precise characterization of somatic complex structural variations from tumor/control paired long-read sequencing data with nanomonsv. *Nucleic Acids Res* **51**, e74 (2023).

Data availability

Sequencing and alignment data:

GIAB HG002 HiFi data publicly available at https://ftp-trace.ncbi.nlm.nih.gov/giab/ftp/data/AshkenazimTrio/HG002_NA24385_son/PacBio_HiFi-Revio_20231031/. HG002 ONT: https://ftp-trace.ncbi.nlm.nih.gov/giab/ftp/data/AshkenazimTrio/HG002_NA24385_son/UCSC_Ultralong_OxfordNanopore_Promethion/. Ashkenazim trio: https://ftp-trace.ncbi.nlm.nih.gov/giab/ftp/data/AshkenazimTrio/. Chinese trio: https://ftp-trace.ncbi.nlm.nih.gov/giab/ftp/data/ChineseTrio/. HG008 HiFi: https://ftp-trace.ncbi.nlm.nih.gov/giab/ftp/data_somatic/HG008/Liss_lab/PacBio_Revio_20240125/. HG008 Illumina: https://ftp-trace.ncbi.nlm.nih.gov/giab/ftp/data_somatic/HG008/Liss_lab/BCM_Illumina-WGS_20240313/. HCC_{1395} and C-OLO829: https://www.pacb.com/connect/datasets/. 20 HPRC samples: https://s3-us-west-2.amazonaws.com/human-pangenomics/index.html?prefix=working/HPRC/.

Benchmark dataset:

HG002 genome wide: https://ftp-trace.ncbi.nlm.nih.gov/ReferenceSamples/giab/release/AshkenazimTrio/HG002_NA24385_son/NIST_SV_v0.6/. HG002 medical regions: https://ftp-trace.ncbi.nlm.nih.gov/ReferenceSamples/giab/release/AshkenazimTrio/HG002_NA24385_son/CMRG_v1.00/. Rare SV: https://github.com/hall-lab/sv_paper_042020/blob/master/Supplementary_File_1.zip. Repeats region: https://genome.ucsc.edu/cgi-bin/hgTables. HGSVC3: https://ftp.1000genomes.ebi.ac.uk/vol1/ftp/data_collections/HGSVC3/release/Variant_Calls/1.0/GRCh38/. HG008: https://ftp-trace.ncbi.nlm.nih.gov/ReferenceSamples/giab/data_somatic/HG008/Liss_lab/analysis/NIST_HG008-T_somatic-stvar_DraftBenchmark_V0.3-20250220/. Consensus benchmark set of HCC_{1395}: https://static-content.springer.com/esm/art%3A1

767 0.1186%2Fs13059-022-02816-6/MediaObjects/13059_2022_2816_MOESM4_ESM.xlsx. Va
768 lidation benchmark set of HCC_{1395}: https://static-content.springer.com/esm/art%3A10.118
769 6%2Fs13059-022-02816-6/MediaObjects/13059_2022_2816_MOESM5_ESM.xlsx. Validati
770 on benchmark set of COLO829: http://doi.org/10.5281/zenodo.4716169.
771 Reference genome:
772 GRCh38: http://ftp.1000genomes.ebi.ac.uk/vol1/ftp/technical/reference/GRCh38_reference_
773 genome/. GRCh37: http://ftp-trace.ncbi.nih.gov/1000genomes/ftp/technical/reference/phase2
774 _reference_assembly_sequence/hs37d5.fa.gz. GRCh38-90c.r518 and GRCh37-91c.r559: ht
775 tps://zenodo.org/records/10693675.

776 Code availability

777 Source code and benchmark scripts for SVPG is available at available at https://github.
778 com/coopsor/SVPG.

779 Author contributions

780 G.W. conceived and managed the work. H.H. and T.J. designed the method, and H.H.
781 implemented it. R.G., Z.J., and S.C. contributed to the experimental evaluations. Y.L., M.Z.,
782 W.G., and S.Z. contributed to data visualization and interpretation. H.H. and T.J. drafted the
783 manuscript. All authors reviewed, revised, and approved the final version of the manuscript.

784 Competing interests

785 The authors declare no competing interests.

786 Acknowledgements

787 This work has been partially supported by the National Natural Science Foundation of
788 China (62225109, 62472120), the National Key R&D Program of China (2024YFC340
789 6303).